



Providing Choice & Value
Generic CT and MRI Contrast Agents

**FRESENIUS
KABI**

CONTACT REP

AJNR










This information is current as
of July 15, 2025.

**DSC Perfusion MRI–Derived Fractional
Tumor Burden and Relative CBV
Differentiate Tumor Progression and
Radiation Necrosis in Brain Metastases
Treated with Stereotactic Radiosurgery**

F. Kuo, N.N. Ng, S. Nagpal, E.L. Pollom, S. Soltys, M.
Hayden-Gephart, G. Li, D.E. Born and M. Iv

AJNR Am J Neuroradiol published online 28 April 2022
<http://www.ajnr.org/content/early/2022/04/28/ajnr.A7501>

DSC Perfusion MRI–Derived Fractional Tumor Burden and Relative CBV Differentiate Tumor Progression and Radiation Necrosis in Brain Metastases Treated with Stereotactic Radiosurgery

 F. Kuo,  N.N. Ng,  S. Nagpal,  E.L. Pollom,  S. Soltys,  M. Hayden-Gephart,  G. Li,  D.E. Born, and  M. Iv



ABSTRACT

BACKGROUND AND PURPOSE: Differentiation between tumor and radiation necrosis in patients with brain metastases treated with stereotactic radiosurgery is challenging. We hypothesized that MR perfusion and metabolic metrics can differentiate radiation necrosis from progressive tumor in this setting.

MATERIALS AND METHODS: We retrospectively evaluated MRIs comprising DSC, dynamic contrast-enhanced, and arterial spin-labeling perfusion imaging in subjects with brain metastases previously treated with stereotactic radiosurgery. For each lesion, we obtained the mean normalized and standardized relative CBV and fractional tumor burden, volume transfer constant, and normalized maximum CBF, as well as the maximum standardized uptake value in a subset of subjects who underwent FDG-PET. Relative CBV thresholds of 1 and 1.75 were used to define low and high fractional tumor burden.

RESULTS: Thirty subjects with 37 lesions (20 radiation necrosis, 17 tumor) were included. Compared with radiation necrosis, tumor had increased mean normalized and standardized relative CBV ($P = .002$) and high fractional tumor burden (normalized, $P = .005$; standardized, $P = .003$) and decreased low fractional tumor burden (normalized, $P = .03$; standardized, $P = .01$). The area under the curve showed that relative CBV (normalized = 0.80; standardized = 0.79) and high fractional tumor burden (normalized = 0.77; standardized = 0.78) performed the best to discriminate tumor and radiation necrosis. For tumor prediction, the normalized relative CBV cutoff of ≥ 1.75 yielded a sensitivity of 76.5% and specificity of 70.0%, while the standardized cutoff of ≥ 1.75 yielded a sensitivity of 41.2% and specificity of 95.0%. No significance was found with the volume transfer constant, normalized CBF, and standardized uptake value.

CONCLUSIONS: Increased relative CBV and high fractional tumor burden (defined by a threshold relative CBV of ≥ 1.75) best differentiated tumor from radiation necrosis in subjects with brain metastases treated with stereotactic radiosurgery. Performance of normalized and standardized approaches was similar.

ABBREVIATIONS: ASL = arterial spin-labeling; AUC = area under the curve; DCE = dynamic contrast-enhanced; FTB = fractional tumor burden; K^{trans} = volume transfer constant; max = maximum; nCBF = normalized CBF; nRCBV = normalized relative CBV; RCBV = relative CBV; RN = radiation necrosis; sRCBV = standardized relative CBV; SRS = stereotactic radiosurgery; SUV = standardized uptake value

Perfusion and metabolic imaging markers such as relative CBV (RCBV) acquired with DSC, volume transfer constant (K^{trans})

acquired with dynamic contrast-enhanced (DCE) imaging, CBF acquired with arterial spin-labeling (ASL), and standardized uptake value (SUV) acquired with [^{18}F] FDG-PET have been investigated to overcome the diagnostic challenge of differentiating progressive tumor and radiation necrosis (RN) in the post-treatment brain tumor setting.^{1–3} A relatively newly described DSC-derived metric, fractional tumor burden (FTB), which is defined as the volume fraction of contrast-enhancing voxels above or below a defined RCBV threshold, has also shown increasing potential for spatial discrimination of tumor and treatment effect.²


Single quantitative perfusion values (such as mean, median, or maximum RCBV) may not accurately reflect the spatial heterogeneity of tumor. FTB, however, can provide per-voxel assessment

Received December 2, 2021; accepted after revision March 14, 2022.

From the Department of Radiology, Division of Neuroimaging and Neurointervention (F.K., N.N.N., M.I.), and Departments of Neurology (Neuro-Oncology) (S.N.), Radiation Oncology (E.L.P., S.S.), Neurosurgery (M.H.-G., G.L.), and Pathology (D.E.B.), Stanford University, Stanford, California.

Frank Kuo and Nathan N. Ng are co-first authors and contributed equally to this work.

Please address correspondence to Michael Iv, MD, Stanford University, Center for Academic Medicine, Radiology + MC: 5659, Room 323A, 453 Quarry Rd, Palo Alto, CA 94304; e-mail: miv@stanford.edu; @Michael_Iv_MD

 Indicates article with online supplemental data.

<http://dx.doi.org/10.3174/ajnr.A7501>

of the entire contrast-enhancing lesion volume. While a previous study used 1 RCBV threshold in the evaluation of tumor,³ we have recently shown, in a study of recurrent glioblastoma, that 2 normalized RCBV thresholds (1 and 1.75) can classify voxels into low- and high-FTB classes, which define fractions of the contrast-enhancing volume with low and high blood volume, respectively, and can help differentiate treatment necrosis from tumor as well as guide clinical decision-making.⁴ Therefore, FTB maps allow spatial representation of areas of suspected tumor and treatment effect, because both can coexist in various proportions within a given lesion.^{2,3} Standardization of RCBV, which uses a method to transform RCBV maps to a standardized intensity scale without the need for operator-defined reference ROIs (potentially minimizing variability in the acquisition of RCBV measurements),⁵ has also shown performance similar to that of normalized RCBV in distinguishing tumor from treatment effect.⁶

In this study, we evaluated the utility of DSC-derived FTB in patients with brain metastases after previous treatment with stereotactic radiosurgery (SRS). We hypothesized that the use of 2 RCBV thresholds (using normalized and standardized approaches) to define low and high FTB, as in our prior study of recurrent glioblastoma,⁴ could be effective in distinguishing progressive tumor from RN in previously treated brain metastases. In this study, RCBV refers to either normalized or standardized RCBV, while nRCBV and sRCBV refer specifically to normalized and standardized RCBV, respectively. A secondary goal was to evaluate the performance of metrics derived from other perfusion and metabolic techniques, including DCE, ASL, and FDG-PET.

MATERIALS AND METHODS

Subjects

This retrospective study was approved by Stanford University's institutional review board. Through a key word search of our PACS database, we identified subjects with brain metastases previously treated with SRS between May 2018 to October 2020. Inclusion criteria were the following: 18 years of age or older, history of brain metastases previously treated with SRS, and post-treatment perfusion MR imaging showing at least 1 suspicious contrast-enhancing lesion (defined by interval growth post-SRS), with the longest lesion diameter measuring ≥ 10 mm. Subjects were excluded if they had nonenhancing lesions, extensive susceptibility related to blood or surgical material (obscuring $>50\%$ of the target lesion) on raw precontrast DSC images, a histopathologic diagnosis of lymphoma or a primary brain tumor such as glioma, or if a clinical assessment of the lesion ground truth could not be established at the time of the study. In a subset of patients who had PET-MR imaging, evaluation of the presence of metabolic activity was performed. Clinical demographics, histopathologic information, and treatment history were obtained through the electronic medical record.

Imaging Acquisition

MRIs were performed on 3T scanners (Discovery MR750 or Signa Architect, GE Healthcare, $n = 28$; Magnetom Skyra, Siemens, $n = 2$). Most imaging was acquired as part of the RN protocol of our institution, which consisted of the following sequences (in order of acquisition): gadolinium 3D T1-weighted inversion recovery fast-

spoiled gradient recalled, ASL, DCE, T2-weighted, DSC, and post-gadolinium 3D T1 inversion recovery fast-spoiled gradient recalled.

ASL imaging (TR/TE = 4000/10 ms, in-plane spatial resolution = 3 mm, section thickness = 4 mm, skip = 0 mm, with the labeling plane at the level of the foramen magnum) was performed with a 3D background-suppressed fast spin-echo technique without vascular suppression using a pseudocontinuous labeling time of 1.5 seconds, followed by a 2-second postlabeling delay.

DCE imaging consisted of 5 axial 3D fast-spoiled gradient recalled flip angle series (2° , 5° , 10° , 15° , and 20°) used for T1 mapping, followed by acquisition of the dynamic images (TR/TE = 3–5/1–2 ms, flip angle = 30° , section thickness = 3 mm with 0-mm skip, FOV = 240 mm, matrix = 128×128 mm, 70 phases, 20 slices/phase, 4 seconds/phase) obtained after the intravenous injection of 0.05 mmol/kg of gadobenate dimeglumine (MultiHance; Bracco Diagnostics). This initial contrast load served as a preload dose to help correct for leakage effects in subsequent DSC imaging. Following DCE and T2-weighted acquisitions, a second 0.05-mmol/kg gadolinium dose was administered for DSC (TR/TE = 1800/35–40 ms, section thickness = 5 mm with 0 mm skip with 20 images covering the brain, flip angle = 60° , matrix = 128×128 mm, FOV = 240 mm). If DCE was not acquired, a dose of 0.05 mmol/kg of gadolinium was still administered as a preload dose before T2-weighted and DSC imaging.

A subset of subjects underwent FDG-PET imaging on a 3T PET-MRI scanner (Signa) using TOF capability, following an intravenous injection of 5–6 mCi of [^{18}F] FDG. The time from injection to imaging was 45–75 minutes. Attenuation correction was performed with zero TE MRI, using proton density differences to classify soft tissues, air, and bone in the head. While PET data were acquired, axial 3D T1 spoiled gradient-recalled images were acquired for PET attenuation correction, with generation of in-phase, out-of-phase, fat, and water images using the Dixon method. In addition, axial proton density-weighted zero TE images (TR/TE = 400/0.02 ms, FOV = 264 mm, matrix = 110×110 mm, section thickness = 2.4 mm with 0-mm skip) were acquired.

Image Processing and Analysis

A second-year neuroradiology fellow (F.K.) performed all image segmentation and ROI placement. All ROIs were reviewed, confirmed, and adjusted (if necessary) by a board-certified neuroradiologist with 10 years of brain tumor imaging interpretation and segmentation experience (M.I.). Each lesion was analyzed separately in subjects with >1 lesion.

DSC Processing and Analysis

We used a workstation equipped with OsiriX MD Imaging Software (Version 7.0; <http://www.osirix-viewer.com>) and a FDA-cleared plug-in (IB Neuro, Version 2.0; Imaging Biometrics), which uses established leakage-correction methods, to process perfusion data and calculate RCBV and FTB.^{2,3,7,8} For semiautomated image processing, we used IB Rad Tech (Version 2.0; Imaging Biometrics), a workflow engine that generates quantitative Δ T1 and FTB maps from the IB Delta Suite (Version 2.0; Imaging Biometrics) and IB Neuro plug-ins (Imaging Biometrics), according to a previously described workflow.^{4,8} Normalization was

Table 1: Demographics and clinical information

	RN (<i>n</i> = 20 Lesions)	Tumor (<i>n</i> = 17 Lesions)
Age (mean) (SD) (yr) ^a	65 (8.9)	54 (12.8)
Sex (male/female) ^a	9:8	3:10
Primary tumor ^b		
Lung	10 (50.0%)	3 (17.6%)
Breast	5 (25.0%)	9 (52.9%)
Melanoma	2 (10.0%)	0
Colorectal	2 (10.0%)	0
Tonsillar	1 (5.0%)	0
Sinonasal	0	3 (17.6%)
Ovarian	0	2 (11.8%)
Surgical resection for determination of histopathologic ground truth diagnosis ^b	7 (35.0%)	6 (35.2%)
Interval time between end of radiation and first MR imaging (median) (range) (mo)	24.9 (4–109)	16.3 (3–41)
Interval time between end of radiation and PET-MR imaging (median) (range) (mo) ^c	27.9 (14–117)	12.4 (6–37)
Total radiation dosage (mean) (SD) (Gy)	24.5 (4.2)	22.8 (3.1)

^a Thirty subjects who had a total of 37 lesions (*n* = 20 RN; *n* = 17 tumor) were included in age and sex analyses.

^b Percentages for primary tumor type and surgical resection are relative to the total number of lesions within each column.

^c Subset of 17 subjects who had a total of 20 lesions (*n* = 8 RN, *n* = 12 tumor) who underwent PET-MRI.

performed relative to the contralateral normal-appearing white matter. Standardization was built into the software algorithm and did not require additional operator-defined input. For each approach, we used 2 previously tested RCBV thresholds (1 and 1.75) to define 3 FTB classes: FTB_{low}, percentage of contrast-enhancing voxels with RCBV of ≤ 1.0 ; FTB_{mid}, percentage of voxels with RCBV between 1.0 and 1.75; and FTB_{high}, percentage of voxels with RCBV of ≥ 1.75 . An sRCBV of 1.56 was also evaluated as a threshold for tumor, given a prior report of this value indicating >88% probability of tumor.^{3,9} Percentage values from the 3 FTB classes were summed to 100%. Mean nRCBV and sRCBV values of the contrast-enhanced volumes were generated for each subject. Contrast-enhanced T1-weighted images of the lesion superimposed on the FTB map containing assigned colored voxels for each class (FTB_{low} = blue; FTB_{mid} = yellow; FTB_{high} = red) and a histogram displaying voxels for the contrast-enhancing volume were also generated.

DCE Processing and Analysis

We used OsiriX MD (Version 7.0) and a commercially available plug-in for DCE analysis (IB DCE, Version 2.0; Imaging Biometrics). Using the semiautomated pipeline of the software, which includes automated generation of the vascular input function, operator-defined segmentation of the entire contrast-enhancing volume on contiguous dynamic contrast-enhanced T1-weighted images, and pharmacokinetic modeling using the 2-compartment Tofts model, we acquired mean K^{trans} values of the contrast-enhancing lesion volume.

ASL and PET Processing and Analysis

Postprocessed ASL imaging was performed by an automated reconstruction script that sent CBF images directly to the PACS.

PET images were reconstructed using TOF ordered subsets expectation maximization (32 subsets, 8 iterations, 256×256 mm matrix, standard z-axis filter, cutoff of 3) and zero TE MRI.

Analysis was performed by manually drawing an ROI around the margin of each enhancing lesion on a single image section that contained the area of maximum enhancement (excluding as

much cystic or necrotic areas as possible) on axial postgadolinium, T1-weighted imaging using OsiriX MD (Version 7.0). The ROI was then transferred to coregistered and postprocessed ASL images to obtain the maximum CBF value and coregistered MRI-based attenuation-corrected FDG-PET images calculated from the PET 45- to 75-minute summed raw data to obtain the maximum standardized uptake value (SUV_{max}). Studies have shown that SUV_{max} is a more reliable and accurate parameter for quantification.¹⁰ SUV_{max} ratios were then produced by normalizing the SUV maps to the pons, which was chosen as a reference area because its metabolism and volume are least affected by disease.¹¹ For consistency, the CBF_{max} of the lesion was also used for ASL, similar to use in prior studies of quantification,¹² and normalized to the pons to obtain the maximum normalized CBF value (nCbf).

Determination of Ground Truth Diagnoses

The diagnosis of tumor was based on fulfilling one of the following criteria: 1) final histopathologic diagnosis in the electronic medical record if the patient underwent resection (*n* = 6); 2) clinical determination by a radiation oncologist (S.S. and E.L.P.) of a tumor-progression diagnosis and need for further treatment (ie, repeat SRS or whole-brain radiation therapy or a CNS-penetrating systemic agent) (*n* = 3); and 3) a decreased contrast-enhancing size of the lesion after repeat SRS, performed after the study perfusion MR imaging (*n* = 8). The diagnosis of RN was based on fulfilling one of the following criteria: 1) final histopathologic diagnosis in the electronic medical record if the patient underwent resection (*n* = 7); and 2) clinical determination by a radiation oncologist (S.S. and E.L.P.) of an RN diagnosis without the need for further treatment (ie, the lesion became smaller on serial MR imaging without tumor-directed therapy, *n* = 13).

For FTB-histopathology correlation, a neuropathologist with >25 years of experience (D.E.B.) evaluated H&E stains of all submitted specimens (mean, 2; range, 1–5) in each subject who had undergone surgical resection. Percentages of tumor and necrosis/gliosis were visually estimated in each specimen. In subjects with

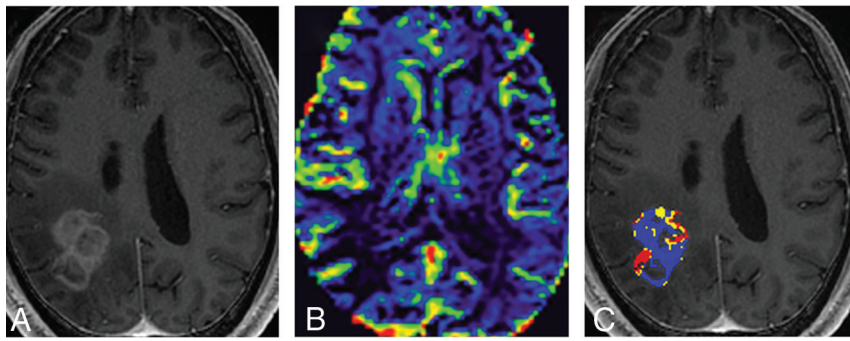


FIG 1. RN in a 58-year-old man with metastatic colon cancer presenting 17 months after surgical resection of a right parietal metastasis treated with SRS. A, Recurrent contrast-enhancing lesion at the site of the original tumor on axial T1-weighted postcontrast image. On DSC, the masslike lesion shows low RCBV (B) and predominantly FTB_{low} (blue) voxels (C). Low perfusion is consistent with pathology-proved RN (with $<5\%$ viable tumor cells).

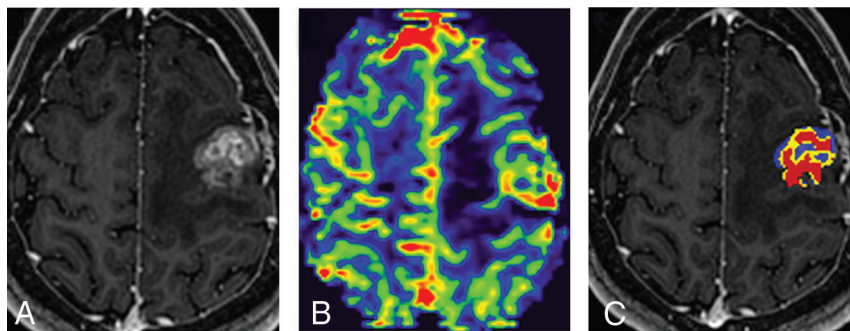


FIG 2. Progressive tumor in a 33-year-old woman with breast cancer presenting 8 months after surgical resection of a left frontal metastasis treated with stereotactic radiosurgery. A, A recurrent contrast-enhancing lesion at the site of the original tumor on an axial T1-weighted postcontrast image. On DSC, the masslike lesion shows high RCBV (B) and predominantly FTB_{high} (red) voxels (C). High perfusion is consistent with pathology-proved progressive tumor.

>1 specimen, percentages of tumor and necrosis/gliosis were obtained by taking the average across all submitted specimens.

Statistical Analyses

Descriptive statistics were used to report demographics, clinical information, and perfusion metrics. We used the non-parametric Mann-Whitney test to compare nRCBV and sRCBV, FTB (using nRCBV and sRCBV threshold values of 1 and 1.75), nCBF, K^{trans} , SUV, and $\Delta T1$ between the tumor and RN groups. The performance of each of these metrics to distinguish tumor from RN was evaluated with the area under the curve (AUC). Sensitivity, specificity, positive predictive value, and negative predictive value were determined for all tumor RCBV thresholds used in the study with MedCalc (Version 20.013; MedCalc Software). A Spearman ρ correlation was used to compare each FTB class with the percentages of tumor burden and necrosis/gliosis (RN) determined by histopathologic examination. $P < .05$ was considered statistically significant for all analyses. Statistical analyses and figures were conducted and created with GraphPad Prism software (Version 9.2.0; GraphPad Software).

RESULTS

Subjects

A total of 39 subjects were initially identified. Subjects were excluded if they had nonenhancing lesions ($n = 3$), extensive susceptibility on raw DSC images ($n = 2$), and a histopathologic diagnosis of lymphoma or other primary brain tumors ($n = 3$). One subject was excluded because a clinical assessment of the lesion ground truth could not be made at the time of the study ($n = 1$). After assessment of eligibility, 30 subjects with a total of 37 brain metastases ($n = 20$ RN, $n = 17$ tumor) were included in the analysis. All subjects underwent the study perfusion MR imaging, comprising DSC ($n = 30$), DCE ($n = 26$), and ASL ($n = 26$). A subset of 17 subjects with 20 total lesions ($n = 8$ RN, $n = 12$ tumor) underwent FDG-PET MR imaging. Table 1 summarizes the demographics and clinicopathologic information. Figures 1 and 2 demonstrate representative DSC imaging performed in subjects with RN and tumor, respectively.

Quantitative FTB and RCBV (DSC)

With the normalized approach, tumor had higher FTB_{high} ($P = .005$) and nRCBV ($P = .002$) and lower FTB_{low} ($P = .03$) than RN (Table 2). No significance was found with FTB_{mid} ($P = .17$). AUCs to differentiate tumor from RN were as follows: 0.71 for FTB_{low} (95% CI, 0.53–0.89; $P = .03$), 0.63 for FTB_{mid} (95% CI, 0.45–0.81; $P = .17$), 0.77 for FTB_{high} (95% CI, 0.60–0.93; $P = .005$), and 0.80 for nRCBV (95% CI, 0.64–0.96; $P = .002$) (Fig 3A and Table 2). For tumor prediction, the nRCBV threshold of ≥ 1.75 yielded a sensitivity of 76.5% and specificity of 70.0%, positive predictive value of 71.8%, and negative predictive value of 74.9% (Table 3).

With the standardized approach, tumor had higher FTB_{high} ($P = .003$) and sRCBV ($P = .002$) and lower FTB_{low} ($P = .01$) compared with RN (Table 2). No significance was found with FTB_{mid} ($P = .89$). AUCs to differentiate tumor from RN were as follows: 0.75 for FTB_{low} (95% CI, 0.57–0.92; $P = .01$), 0.51 for FTB_{mid} (95% CI, 0.32–0.71; $P = .89$), 0.78 for FTB_{high} (95% CI, 0.62–0.95; $P = .003$), and 0.79 for sRCBV (95% CI, 0.63–0.95; $P = .002$) (Fig 3B and Table 2). For tumor prediction, the sRCBV cutoff of ≥ 1.75 yielded a sensitivity of 41.2%, specificity of 95.0%, positive predictive value of 89.2%, and negative predictive value of 61.8% (Table 3). The sRCBV cutoff of ≥ 1.56 yielded similar results, with a sensitivity of 47.1%, specificity of 90.0%, positive predictive value of 82.5%, and negative predictive value of 63.0% (Table 3).

Table 2: Multiparametric perfusion, metabolic, and volumetric values in RN and tumor groups

	Radiation Necrosis ^b	Tumor ^b	P Value ^c	AUC ^d	AUC (95% CI)
DSC					
Normalized RCBV ^a					
FTB _{low} (%)	49.5 (30.1)	28.1 (23.8)	.03 ^e	0.71	0.53–0.89
FTB _{mid} (%)	17.7 (10.8)	13.4 (7.1)	.17	0.63	0.45–0.81
FTB _{high} (%)	32.8 (27.0)	58.6 (24.1)	.005 ^e	0.77	0.60–0.93
nRCBV	1.51 (0.9)	2.92 (1.5)	.002 ^e	0.80	0.64–0.96
Standardized RCBV ^a					
FTB _{low} (%)	62.6 (26.2)	33.8 (16.1)	.01 ^e	0.75	0.57–0.92
FTB _{mid} (%)	21.6 (15.7)	22.8 (7.2)	.89	0.51	0.32–0.71
FTB _{high} (%)	15.9 (14.0)	43.3 (20.9)	.003 ^e	0.78	0.62–0.95
sRCBV	0.94 (0.50)	1.63 (0.82)	.002 ^e	0.79	0.63–0.95
DCE					
K ^{trans} (min ⁻¹)	0.02 (0.02)	0.03 (0.04)	.23	0.64	0.43–0.85
ASL					
nCBF	1.25 (0.42)	1.67 (0.68)	.05	0.71	0.52–0.90
FDG-PET MR imaging					
SUV	1.33 (0.19)	1.62 (0.43)	.15	0.69	0.46–0.93
Volumetrics					
Δ T1 (cm ³)	3.24 (4.58)	3.76 (2.60)	.14	0.64	0.46–0.83

^a Thresholds of 1 and 1.75.^b Values for RN and tumor groups are expressed in mean (SD).^c P values obtained from nonparametric Mann-Whitney tests.^d AUC obtained from receiver operating characteristic curves.^e P values are statistically significant.**Quantitative K^{trans} (DCE), nCBF (ASL), SUV (FDG-PET), and Δ T1**

Between RN and tumor, no significance was observed with mean K^{trans} ($P = .23$), nCBF ($P = .05$), SUV ($P = .15$), and Δ T1 ($P = .14$) (Table 2). AUCs for differentiating RN and tumor were as follows: 0.64 for K^{trans} (95% CI, 0.43–0.85; $P = .23$), 0.71 for nCBF (95% CI, 0.52–0.90; $P = .05$), 0.69 for SUV (95% CI, 0.46–0.93; $P = .15$), and 0.64 for Δ T1 (95% CI, 0.46–0.83, $P = .14$) (Fig 3C).

FTB-Histopathology Correlation

Thirteen subjects had surgical resection after the study perfusion MR imaging. However, only 11 subjects ($n = 5$ tumor and $n = 6$ RN) had specimens available for histopathologic analysis in this part of the study. With the normalized approach, no significant correlation was observed with FTB_{low} (versus percentage tumor: $\rho = -0.38$, $P = .25$; versus percentage necrosis/gliosis, $\rho = 0.38$, $P = .25$), FTB_{mid} (versus percentage tumor: $\rho = 0.26$, $P = .43$; versus percentage necrosis/gliosis, $\rho = -0.26$, $P = .43$), and FTB_{high} (versus percentage tumor: $\rho = 0.48$, $P = .13$; versus percentage necrosis/gliosis, $\rho = -0.48$, $P = .13$) (Online Supplemental Data).

With the standardized approach, no significant correlation was observed with FTB_{low} (versus percentage tumor: $\rho = -0.59$, $P = .06$; versus percentage necrosis/gliosis, $\rho = 0.59$, $P = .06$), FTB_{mid} (versus percentage tumor: $\rho = 0.42$, $P = .19$; versus percentage necrosis/gliosis, $\rho = -0.42$, $P = .19$), and FTB_{high} (versus percentage tumor: $\rho = 0.57$, $P = .07$; versus percentage necrosis/gliosis, $\rho = -0.57$, $P = .07$) (Online Supplemental Data).

With both approaches, however, FTB_{high} and FTB_{low} suggested a positive correlation, respectively, with the percentage of tumor and the percentage of necrosis/gliosis (Online Supplemental Data).

DISCUSSION

Our results show that the use of 2 RCBV thresholds (1 and 1.75) to define FTB classes, FTB_{low} and FTB_{high}, allowed differentiation

of tumor and RN in brain metastases following SRS. The performance of normalized and standardized approaches to achieve this task was similar. Additional perfusion and metabolic metrics of K^{trans} (DCE), nCBF (ASL), and SUV (FDG-PET), and Δ T1 did not reliably distinguish tumor from RN.

Results from the current study using 2 nRCBV thresholds (1 and 1.75) in treated brain metastases are similar to results from our previous study of treated recurrent glioblastomas, in which nRCBV and FTB_{high} best differentiated tumor from treatment effect.⁴ The use of 1 as a lower threshold for identifying RN and 1.75 as an upper threshold for identifying progressive tumor in posttreatment brain metastases is close to previously reported RCBV thresholds for differentiation of radiation-related changes (<1.35)¹³ and tumor (range, >2 – 2.1).^{14,15} As previously described, elevated blood volume and FTB_{high} are likely reflective of increased angiogenesis within tumors.⁴ FTB_{low} performed slightly less well because there is likely an overlap between hypovascular tumor and radiation-related coagulative necrosis/gliosis.¹⁶ FTB_{mid}, which includes all RCBV values between 1 and 1.75, did not reliably differentiate RN from tumor because there is likely an admixture of both in varying proportions within this range of values. Additionally, normalized and standardized RCBV and FTB approaches performed similarly, consistent with a recent study in high-grade gliomas.⁶ However, there was a trade-off in the sensitivity and specificity between the 2 approaches when using the ≥ 1.75 RCBV threshold for tumor prediction, possibly related to differences in postprocessing techniques (eg, the reference ROI in the contralateral normal-appearing white matter is required for normalization and not for standardization) and intrasubject variations with time.⁷ For tumor prediction, the sensitivity and specificity were similar for the sRCBV cutoff values of ≥ 1.75 and ≥ 1.56 . Nonetheless, standardization of DSC perfusion imaging, because sRCBV requires less operator-defined

Normalized

Standardized

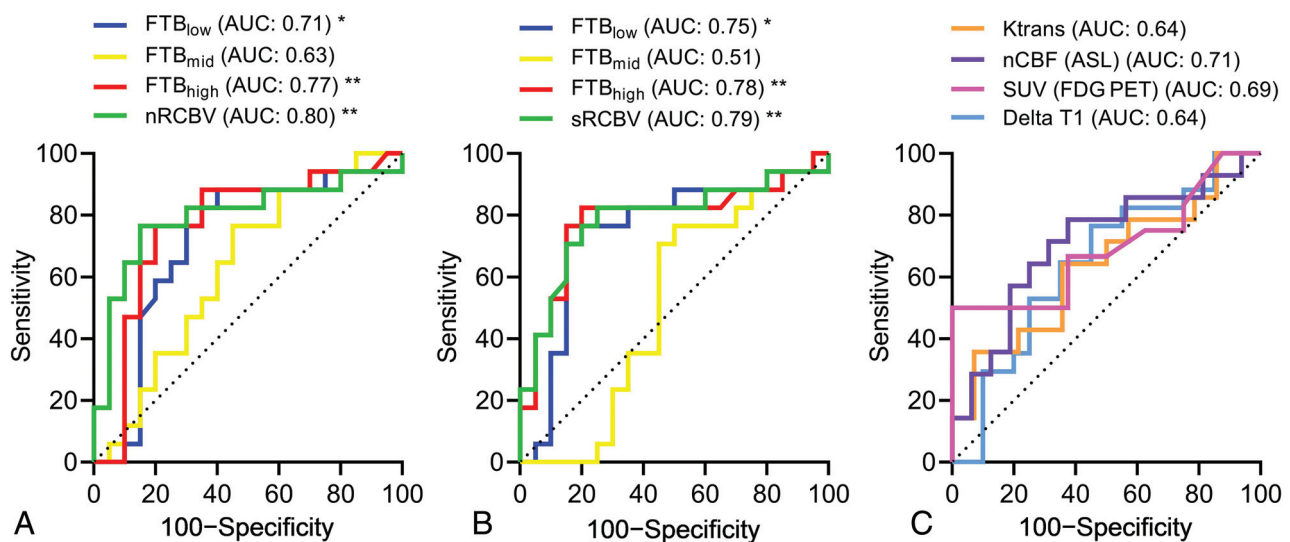


FIG 3. Receiver operating characteristic AUC analyses demonstrate that FTB and RCBV significantly differentiate RN from tumor. A, AUCs of FTB classes and nRCBV to differentiate RN from tumor were 0.71 for FTB_{low} (95% CI, 0.53–0.89; $P = .03$), 0.63 for FTB_{mid} (95% CI, 0.45–0.81; $P = .17$), 0.77 for FTB_{high} (95% CI, 0.60–0.93; $P = .005$), and 0.80 for nRCBV (95% CI, 0.64–0.96; $P = .002$). B, AUCs of FTB classes and sRCBV to distinguish RN and tumor were 0.75 for FTB_{low} (95% CI, 0.57–0.92; $P = .01$), 0.51 for FTB_{mid} (95% CI, 0.32–0.71; $P = .89$), 0.78 for FTB_{high} (95% CI, 0.62–0.95; $P = .003$), and 0.79 for sRCBV (95% CI, 0.63–0.95; $P = .002$). C, AUCs of K^{trans} , nCBF (ASL), SUV (FDG-PET), and Δ T1 to differentiate RN from tumor were 0.64 for K^{trans} (95% CI, 0.43–0.85; $P = .23$), 0.71 for nCBF (ASL) (95% CI, 0.52–0.90; $P = .05$), 0.69 for SUV (FDG-PET) (95% CI, 0.46–0.93; $P = .15$), and 0.64 for Δ T1 (95% CI, 0.46–0.83; $P = .14$). The asterisk and double asterisks denote $P < .05$ and $P < .01$, respectively.

Table 3: Sensitivity, specificity, PPV, and NPV of nRCBV and sRCBV thresholds for prediction of tumor

	Sens	Spec	PPV	NPV
nRCBV (1.75)	76.5	70.0	71.8	74.9
sRCBV (1.75)	41.2	95.0	89.2	61.8
sRCBV (1.56)	47.1	90.0	82.5	63.0

Note:—Sens indicates sensitivity; spec, specificity; PPV, positive predictive value; NPV, negative predictive value.

input than nRCBV, may represent an important step toward greater multicenter adoption and use.

One of the advantages of FTB maps is the potential for spatially mapping coexisting areas of tumor and treatment effect within a given lesion.² High-grade glioma studies using image-localized biopsies within contrast-enhancing lesions have shown that areas with low RCBV and FTB proved to be treatment effect and areas with high RCBV and FTB proved to be tumor on histopathology.^{2,3,6} In our study, though not significant (potentially related to the lower availability of surgical specimens for histopathologic examination), we similarly found a positive correlation between FTB_{high} and the percentage of tumor on histopathology and a positive correlation between FTB_{low} and the percentage of necrosis and gliosis on histopathology. However, additional investigations correlating tumor and necrosis fractions with defined FTB classes are needed for histologic confirmation.

Beyond DSC in our study, metrics of K^{trans} (DCE), nCBF (ASL), and SUV (FDG-PET) did not reliably differentiate tumor and RN, in contrast to other studies.^{1,17,18} Blood flow values derived from ASL and SUV from FDG-PET have shown utility in identifying tumor progression in treated brain metastases, with

an equivalent sensitivity of 83% and a specificity of 100% for ASL and 75% for FDG-PET in 1 study.¹⁹ Suh et al¹ found that the pooled sensitivity and specificity of 5 studies, including the aforementioned study, using FDG-PET to differentiate tumor from RN in post-SRS brain metastases, were 83% and 88%, respectively. Results from our study may differ from those of previously published studies because of differences in our cohorts (eg, types and numbers of included metastatic tumors). Due to the lack of validated thresholds for ASL, DCE, and FDG-PET, we did not perform a combined multimodal or multiparametric analysis, though it has been previously shown in treated glioblastomas that the combination of parameters such as RCBV and K^{trans} can improve the overall diagnostic accuracy in differentiating recurrent tumor and treatment effect (RCBV, 85.8%; K^{trans} , 75.5%; RCBV and K^{trans} , 92.8%).²⁰ In addition, as expected, the use of Δ T1 as a volumetric measurement of gadolinium enhancement did not perform well in predicting tumor response, presumably related to the overlap of gadolinium leakage across a disrupted blood-brain barrier in both tumor and RN.²¹

Our study has important limitations. First, the small sample size consisting of retrospective data from a single institution limits the generalizability of our results. Second, we included various types of tumor histology in our analysis. Brain metastases have been shown to have different tumor perfusion values depending on the primary cancer type, with brain metastases derived from renal cell carcinoma and melanoma typically having higher RCBV values than those derived from lung, breast, and gastrointestinal tumors.²² Our subject cohort consisted primarily of lung- and breast-derived lesions, possibly accounting for less striking and prominent differences in tumor

RCBV.²² In addition, not all metastases are hypervascular; 1 study reported variation in tumor blood flow even between metastases derived from the same primary carcinoma, with approximately 40% of metastases overall showing blood flow less than or equivalent to blood flow from contralateral healthy cortex.¹⁸ In these cases, perfusion MR imaging alone may not be sufficiently sensitive to distinguish tumor growth and RN. In future studies, it may be helpful to establish baseline pretreatment values for comparison with posttreatment values or to combine perfusion imaging with other modalities, depending on the primary tumor histology.^{17,18}

Additionally, given the heterogeneity in tumor origin in studies of RN, it may be warranted in a future study to systematically stratify diagnostic accuracies of brain metastases according to tumor histology. Third, while we excluded lesions with blood products obscuring >50% of the lesion, metastases with minor blood products were still included in DSC analysis. This limitation is reflective of real-time clinical practice because blood products are common in post-SRS lesions. It may also underscore the use of other perfusion parameters and techniques to help with interpretation. Fourth, we did not have image-localized biopsy tissue from the 3 distinct FTB classes evaluated, limiting the direct per-voxel comparison of perfusion imaging metrics with fractions of tumor and necrosis present on histopathology.

CONCLUSIONS

DSC-derived FTB using nRCBV or sRCBV thresholds of 1 and 1.75 can provide per-voxel analysis of low and high blood volume and can differentiate progressive tumor from RN in brain metastases previously treated with SRS. Normalized and standardized approaches achieve similar performance for this task, though sRCBV may have the potential for better reproducibility across time and sites. Additional metrics of K^{trans} (DCE), nCBF (ASL), SUV (FDG-PET), and ΔT_1 did not reliably differentiate tumor from RN. Nonetheless, the evaluated RCBV thresholds and FTB classes in this study require further clinical and histologic validation in larger prospective studies.

Disclosure forms provided by the authors are available with the full text and PDF of this article at www.ajnr.org.

REFERENCES

1. Suh CH, Kim HS, Jung SC, et al. **Comparison of MRI and PET as potential surrogate endpoints for treatment response after stereotactic radiosurgery in patients with brain metastasis.** *AJR Am J Roentgenol* 2018;211:1332–41 [CrossRef Medline](#)
2. Hu LS, Eschbacher JM, Heiserman JE, et al. **Reevaluating the imaging definition of tumor progression: perfusion MRI quantifies recurrent glioblastoma tumor fraction, pseudoprogression, and radiation necrosis to predict survival.** *Neuro Oncol* 2012;14:919–30 [CrossRef Medline](#)
3. Prah MA, Al-Gizawi MM, Mueller WM, et al. **Spatial discrimination of glioblastoma and treatment effect with histologically-validated perfusion and diffusion magnetic resonance imaging metrics.** *J Neurooncol* 2018;136:13–21 [CrossRef Medline](#)
4. Iv M, Liu X, Lavezo J, et al. **Perfusion MRI-based fractional tumor burden differentiates between tumor and treatment effect in recurrent glioblastomas and informs clinical decision-making.** *AJNR Am J Neuroradiol* 2019;40:1649–57 [CrossRef Medline](#)
5. Bedekar D, Jensen T, Schmainda KM. **Standardization of relative cerebral blood volume (rCBV) image maps for ease of both inter- and inpatient comparisons.** *Magn Reson Med* 2010;64:907–13 [CrossRef Medline](#)
6. Hoxworth JM, Eschbacher JM, Gonzales AC, et al. **Performance of standardized relative CBV for quantifying regional histologic tumor burden in recurrent high-grade glioma: comparison against normalized relative CBV using image-localized stereotactic biopsies.** *AJNR Am J Neuroradiol* 2020;41:408–15 [CrossRef Medline](#)
7. Prah MA, Stufflebeam SM, Paulson ES, et al. **Repeatability of standardized and normalized relative CBV in patients with newly diagnosed glioblastoma.** *AJNR Am J Neuroradiol* 2015;36:1654–61 [CrossRef Medline](#)
8. Schmainda KM, Prah MA, Hu LS, et al. **Moving toward a consensus DSC-MRI protocol: validation of a low-flip angle single-dose option as a reference standard for brain tumors.** *AJNR Am J Neuroradiol* 2019;40:626–63 [CrossRef Medline](#)
9. Connelly JM, Prah MA, Santos-Pinheiro F, et al. **Magnetic resonance imaging mapping of brain tumor burden: clinical implications for neurosurgical management: case report.** *Neurosurgery Open* 2021;2:okab029 [CrossRef Medline](#)
10. Ulaner GA. Measuring treatment response on FDG PET/CT. In: Ulaner GA. *Fundamentals of Oncologic PET/CT*. Elsevier; 2019:225–29
11. Minoshima S, Frey KA, Foster NL, et al. **Preserved pontine glucose metabolism in Alzheimer disease: a reference region for functional brain image (PET) analysis.** *J Comput Assist Tomogr* 1995;19:541–47 [CrossRef Medline](#)
12. Delgado AF, De Luca F, Hanagandi P, et al. **Arterial spin-labeling in children with brain tumor: a meta-analysis.** *AJNR Am J Neuroradiol* 2018;39:1536–42 [CrossRef Medline](#)
13. Barajas RF, Chang JS, Sneed PK, et al. **Distinguishing recurrent intra-axial metastatic tumor from radiation necrosis following gamma knife radiosurgery using dynamic susceptibility-weighted contrast-enhanced perfusion MR imaging.** *AJNR Am J Neuroradiol* 2009;30:367–72 [CrossRef Medline](#)
14. Sawlani V, Davies N, Patel M, et al. **Evaluation of response to stereotactic radiosurgery in brain metastases using multiparametric magnetic resonance imaging and a review of the literature.** *Clin Oncol (R Coll Radiol)* 2019;31:41–49 [CrossRef Medline](#)
15. Hoefnagels FW, Lagerwaard FJ, Sanchez E, et al. **Radiological progression of cerebral metastases after radiosurgery: assessment of perfusion MRI for differentiating between necrosis and recurrence.** *J Neurol* 2009;256:878–87 [CrossRef Medline](#)
16. Barajas R Jr, Chang JS, Segal MR, et al. **Differentiation of recurrent glioblastoma multiforme from radiation necrosis after external beam radiation therapy with dynamic susceptibility-weighted contrast-enhanced perfusion MR imaging.** *Radiology* 2009;253:486–96 [CrossRef Medline](#)
17. Knitter JR, Erly WK, Stea BD, et al. **Interval change in diffusion and perfusion MRI parameters for the assessment of pseudoprogression in cerebral metastases treated with stereotactic radiation.** *AJR Am J Roentgenol* 2018;211:168175 [CrossRef Medline](#)
18. Lambert EA, Holmes S. **Differentiating radiation-induced necrosis from tumor progression after stereotactic radiosurgery for brain metastases, using evaluation of blood flow with arterial spin labeling (ASL): the importance of setting a baseline.** *Acta Neurochir Suppl* 2021;128:113–19 [CrossRef Medline](#)
19. Lai G, Mahadevan A, Hackney D, et al. **Diagnostic accuracy of PET, SPECT, and arterial spin-labeling in differentiating tumor recurrence from necrosis in cerebral metastasis after stereotactic radiosurgery.** *AJNR Am J Neuroradiol* 2015;36:2250–55 [CrossRef Medline](#)
20. Nael K, Bauer AH, Hormigo A, et al. **Multiparametric MRI for differentiation of radiation necrosis from recurrent tumor in patients with treated glioblastoma.** *AJR Am J Roentgenol* 2018;210:18–23 [CrossRef Medline](#)
21. Iv M, Bisdas S. **Neuroimaging in the era of the evolving WHO Classification of Brain Tumors, From the AJR Special Series on Cancer Staging.** *AJR Am J Roentgenol* 2021;217:3–15 [CrossRef Medline](#)
22. Zhang H, Zhang G, Oudkerk M. **Brain metastases from different primary carcinomas: an evaluation of DSC MRI measurements.** *Neuroradiol J* 2012;25:67–75 [CrossRef Medline](#)